

## Original Article

# Establishment and clinical value of a circulating tumor cell system based on a multi-site immune lipid magnetic sphere technique in laryngopharyngeal head and neck tumors

Wei Chen<sup>1</sup>, Qin Lin<sup>1</sup>, Desheng Wang<sup>1</sup>, Wenting Xie<sup>1</sup>, Chunyan Huang<sup>1</sup>, Wenjing Fan<sup>1</sup>, Shipu Wu<sup>2</sup>, Xiaomei Fan<sup>2</sup>, Chen Li<sup>1</sup>

<sup>1</sup>Department of Otolaryngology, Fujian Medical University Union Hospital, Fuzhou 350001, Fujian, China;

<sup>2</sup>Department of ENT, Zhenghe County Hospital, Nanping 353605, Fujian, China

Received July 30, 2024; Accepted January 3, 2025; Epub January 15, 2025; Published January 30, 2025

**Abstract:** This study aimed to construct multi-site magnetic nanospheres to capture circulating tumor cells (CTCs) from peripheral blood specimens of laryngopharyngeal head and neck tumors. Separated CTCs were used to measure downstream molecular markers and to detect and analyze the disease status. A stable CTC multisite nano-enrichment system was used to determine changes in CTCs levels in Programmed Death-Ligand-1 (PD-L1)-positive patients and to assess the extent of real-time changes in CTCs over the course of the disease in correlation with clinicopathological indicators. The results demonstrated that the constructed immunomagnetic spheres could effectively capture CTCs and that the constructed lipid nanoparticles exhibited high capture efficiency and low cytotoxicity. The results of the concordance or complementarity analyses of PD-L1 expression at the CTC and tissue levels indicated good concordance between the two at up to 70%. The analysis of PD-L1 expression and the changes in CTCs in PD-L1-positive cells plays an auxiliary role in clinical diagnosis and can be used as a dynamic detection index for the course of head, neck, and throat tumor treatment and as a predictor of recurrence risk.

**Keywords:** Laryngopharyngeal head and neck tumors, PD-L1, CTCs, tumor dynamic detection, predictive factors

## Introduction

Head and neck cancer is the sixth most common cancer worldwide and primarily includes oral, nasopharyngeal, oropharyngeal, laryngeal, and hypopharyngeal cancers [1, 2]. Most patients typically present with local lesions at diagnosis and progress to advanced stages. Tumor heterogeneity is the main cause of differences and failures in tumor-targeted therapy and immunotherapy responses [3-6]. Additionally, tumor recurrence or distal metastasis caused by lymph node infiltration often leads to poor prognosis, and the 5-year survival rate of patients remains < 50% [7]. In recent years, tumor immunotherapy has developed rapidly. Commonly used clinical immunotherapy methods include immune vaccines, immune checkpoint inhibitor (ICI) therapy, adoptive immune cell therapy, cytokine therapy, and others

[8-10]. Treatment with immune checkpoint inhibitors can significantly improve the prognosis of patients with advanced cancer. ICI therapy has gained considerable attention in recent years. However, the proportion of patients responding to ICI therapy is not high [11]. This suggests that there is an urgent need for research to understand the high heterogeneity of tumors, the complexity of tumor formation, and the application of this information in the context of clinical practice.

Circulating tumor cells (CTCs) are tumor cells released from solid tumors or metastatic sites and enter the blood circulation, where they travel through the bloodstream to reach distant organs [12-14]. CTCs propagate from the primary site and acquire a more aggressive phenotype and metastatic capacity through epithelial-mesenchymal transition (EMT), and this

reflects the real-time status of the tumor genotype that exhibits a high degree of genetic heterogeneity in patients [15, 16]. Therefore, the analysis of individual CTCs is helpful for elucidating tumor heterogeneity and analyzing the overall picture of genomic mutations during the tumor process [17, 18]. The main technical difficulty in conventional CTC capture research is that the number of CTCs in body fluids (e.g., blood) is very low [19]. In this study, we attempted to separate and enrich the number of tumor cells using multi-site immune magnetic nanoparticles and accurately analyzed the number of cells in body fluids, with good repeatability and specificity [20, 21]. CTCs also exhibit better consistency and specificity than other blood tests such as serum tumor markers [22-24]. CTC-based approaches can be used in the diagnosis and prognostic assessment of metastatic breast, colorectal, lung, and prostate cancer [25-27].

Programmed Death-Ligand-1 (PD-L1) is a common molecular marker in tumor cells that facilitates immune escape and has proven to be a key breakthrough in immunotherapy [28]. Certain investigators have reported high PD-L1 expression in tumor cells of breast cancer patients, and similar results were observed in chronic lymphocytic leukemia, certain types of T/B-cell lymphomas, and gastric, esophageal, kidney, breast, and bladder cancers [29-35]. In light of these reports detailing the correlation of PD-L1 expression with lymph node metastasis, tumor stage, and survival, we explored the value of PD-L1 in head, neck, and throat tumors to assess the risk of recurrence and metastasis. We aimed to determine the clinical significance of CTCs in patients with malignancies treated with PD-L1 immunotherapy by combining CTC and PD-L1 markers.

Our cell sorting system is based on the CellSearch system using a single anti-epithelial Cell Adhesion Molecule (EpCAM)-modified magnetic bead [36] combined with the addition of two other antibodies that include vimentin and epithelial growth factor receptor (EGFR). This system can be used to establish multi-targeted head, neck, and throat tumor CTC-sorting magnetic beads to achieve more comprehensive CTC capture. This study also explored the correlation of PD-L1 positive CTCs captured using

EpCAM, vimentin, and EGFR with the clinicopathology of enrolled patients.

### Materials and methods

#### *Preparation of antibody-modified magnetic liposomes (MLs)*

The immunomagnetic spheres were prepared using the reverse evaporation method. The specific preparation method can be found in literature regarding team cooperation [37]. First, 5 mg each of dioleoyl phosphatidylcholine (DOPC) and cholesterol (Chol) were weighed and added to two 50 mL three-way flasks. Then, 1.0 mL of the oil-soluble  $\text{Fe}_3\text{O}_4$  solution was removed from ethanol and dissolved in 3.0 mL of 1,2-dichloroethane ( $\text{CH}_2\text{Cl}_2$ ), and  $\text{Fe}_3\text{O}_4/\text{CH}_2\text{Cl}_2$  was transferred to the three-mouth flask. The round-bottomed flask was emulsified in an ice bath for 6 min using a probe sonometer, and 2 mg of anti-EpCAM, anti-vimentin, and anti-EGFR antibody derivatives were dissolved into 6 mL of double-steam water ( $\text{ddH}_2\text{O}$ ) and slowly added to the three-mouth flask. After ultrasound treatment, the residual  $\text{CH}_2\text{Cl}_2$  was removed using a rotary evaporation apparatus, and the solution was magnetically separated and washed three times to obtain immunomagnetic microspheres. The methods for constructing the cluster of differentiation 8 (CD8) and CD4 antibody-modified magnetic beads were consistent with those described above.

#### *Characterization of immunomagnetic liposomes (IML)*

The size and zeta potential of the EpCAM/vimentin/EGFR-IMLs were measured using a Zetasizer Nano-ZS 90 (Malvern Instruments Ltd., UK). Atomic force microscopy (AFM) was used to observe the morphology of the nanomagnetic spheres. The hysteresis loops of IMLs were measured using a PPMS-9 instrument (QUANTUM DESIGN, USA). An ultraviolet spectrophotometer was used to scan the ultraviolet absorption peaks of the solution of the nanomagnetic sphere.

#### *Cellular level analysis of the CTC capture system*

*Cell lines:* Head and neck tumor cell lines (HNE1, FaDu, and Hep-2) and the control cell line K562 were purchased from ATCC. DMEM

## CTCs and PD-L1 in laryngopharyngeal head and neck tumors

media, fetal bovine serum (FBS), and trypsin were purchased from Gibco.

### *Analysis of nano magnetic sphere cytotoxicity*

HNE1, FaDu, and Hep-2 head and neck tumor cells used in this study were routinely cultured in DMEM complete culture medium containing 10% fetal bovine serum (FBS) and 1% penicillin-streptomycin. The culture conditions were 37°C and 5% CO<sub>2</sub> under wet conditions. The volume of complete culture medium used for different culture plates was 2 ml for the 35 mm dish, 3 ml for the 60 mm dish, and 8 ml for the 10 cm dish. CCK8 assay was used to determine the *in vitro* cytotoxicity of EpCAM-IML (Ep-IML), vimentin (Vi-IML), and EGFR-IML (EG-IML). Absorbance was measured at 450 nm using a multimode enzyme labeler (Synergy™ HT, BioTek, USA).

### *CTC capture system for clinical sample analysis*

**Sample collection:** This study was conducted in accordance with the principles of the Declaration of Helsinki. This study was approved by the Ethics Committee of Fujian Medical University Union Hospital (2021WSJK011). Peripheral blood samples were collected from patients diagnosed with laryngopharyngeal head and neck cancers at the Department of Otolaryngology, Fujian Medical University Union Hospital. A total of 7.5 mL of peripheral whole blood was collected for counting and analyzing different fractions of CTCs, and clinicopathological data were recorded. Informed consent was obtained from all patients enrolled in the study.

**Reagents:** EpCAM, vimentin, and EGFR monoclonal antibodies were purchased from Abcam. Magnetic nanoparticle-based materials were purchased from Lieyuan Biomedicine Co., Ltd. DAPI staining solution was purchased from Sigma-Aldrich. CD45-PE was purchased from eBioscience. The fluorescence microscope that was used was an OLYMPUS B×61 (Olympus, Japan).

### *Enrichment, fluorescence identification, and counting of peripheral blood CTCs*

Peripheral blood samples were collected from each patient for CTC counts at corresponding

time points. CTCs were enriched and counted using EpCAM/Vimentin/EGFR-nano magnetic spheres. Intact cells with nuclei were identified using the fluorescent nucleic acid dye DAPI, and epithelial cells were distinguished from leukocytes using fluorescent-labeled monoclonal antibodies against CD45 and CK 8, 18, 19 using a multi-color fluorescence cell counter. Evaluation criteria for CTCs were determined. Cells that were FITC+, CK 8, 18, 19+, and DAPI+ were considered CTCs.

### *CTC PD-L1 immunofluorescence assay*

After transmembrane centrifugation, the blood was centrifuged at 1,000 rpm, rinsed with PBS (800-1,000 µL), and transferred to a labeled centrifuge tube. EpCAM, vimentin, and EGFR magnetic spheres were used to capture CTCs. For fluorescence microscopy, 15 µL of DAPI staining solution, 10 µL of CK-FITC staining solution, and 20 µL of PD-L1 Alexa Fluor647 antibody were added to each centrifuge tube and incubated for 30 min in the dark. After incubation, the samples were prepared and then counted by fluorescence microscopy. PD-L1 positive cells exhibited red fluorescence, DAPI exhibits blue fluorescence, and CK-FITC yields green fluorescence.

### *Immunohistochemical analysis of PD-L1*

An appropriate amount of fixed fresh tissue was cleaned with ultrapure water, dehydrated using an alcohol gradient, treated with xylene, and dipped into wax to prepare wax blocks after embedding. The tissue was incubated overnight at 4°C with PD-L1 antibody, and DAB working solution was then applied. Slides were obtained and examined after dehydration with hematoxylin and xylene. PD-L1 expression is brown, and the nuclei stained with DAPI appear blue upon fluorescence microscopy.

### *Statistical analysis*

Data for each group were processed using SPSS 19.0 statistical software. The quantitative data are expressed as mean ± s.d. The rank-sum test was used for statistical analysis. Diagnostic sensitivity, specificity, validity, positive predictive value, and negative predictive value were calculated, and *P-value* < 0.05 was considered statistically significant.

# CTCs and PD-L1 in laryngopharyngeal head and neck tumors

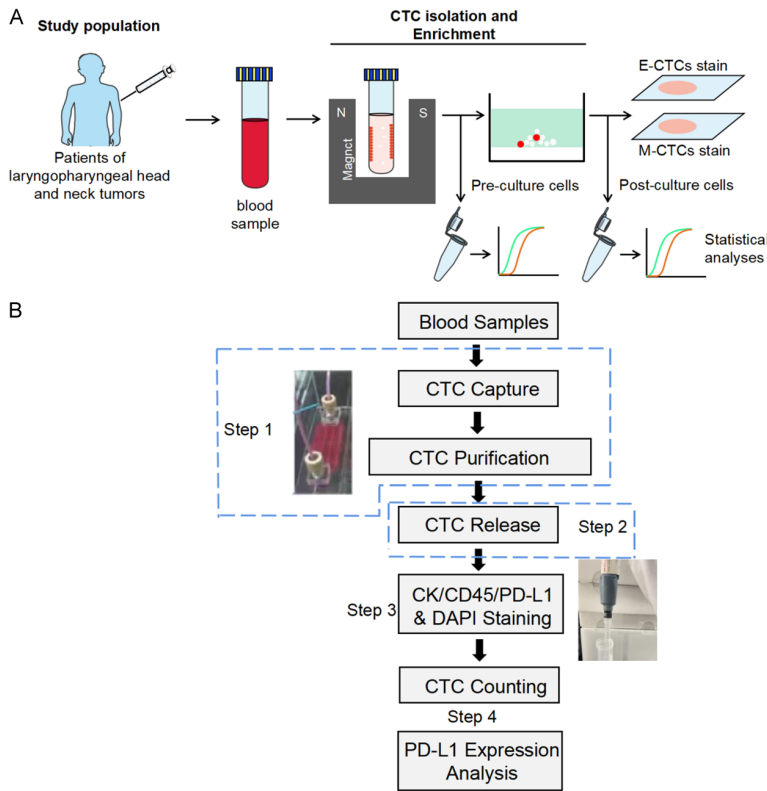


**Figure 1.** Experimental design and flow diagram. A. Peripheral blood collection and CTC enrichment analysis. B. Processing of peripheral blood samples.

## Results

### Preparation of magnetic nanospheres and CTC sorting

The establishment of a CTC enrichment system for head, neck, and throat tumors was carried out according to the principle of antigen-antibody binding, and the preparation process can be referred to the literature report. Briefly, the antibodies (anti-EpCAM, anti-vimentin, and anti-EGFR) were allowed to react with glycidylhexadecyldimethylammonium chloride (GHDC) to form an antibody-GHDC composite derivative in which DOPC was the structural framework, and cholesterol stabilized the lipid molecular layer. The oxidation rate of the liposome-encapsulated  $\text{Fe}_3\text{O}_4$  bare magnetic spheres was slow. This CTC capture platform created for materialistic characterization and analysis was used for the processing and CTC analysis of the patient's peripheral blood. Subsequently, immunofluorescence staining of the isolated CTCs with antibodies, fluorescence microscopy, and statistical analysis of the experimen-

tal results were performed. PD-L1 expression was analyzed in both blood and tissue samples for concordance and complementarity analyses. The overall processes of CTC isolation, CTC count, and PD-L1 expression analysis are presented in **Figure 1A** and **1B**.

### Performance validation and functional evaluation of IML

Ep-IML, Vi-IML, and EG-IML were constructed and characterized materialistically, including particle size, potential, and magnetic saturation curves (**Supplementary Figure 1**). The particle sizes of the constructed CD8 antibody-modified IML (CD8-IML) and CD4 antibody-modified IML (CD4-IML) were tested. The average particle size of CD8-IML was  $177.22 \pm 3.41$  nm with a PDI of 0.118 (**Figure 2A**), and the average particle size of CD4-IML was  $166.31 \pm 4.48$  nm with a PDI of 0.141 (**Figure 2C**). The zeta potential of CD8-IML was  $6.71 \pm 4.16$  mv (**Figure 2B**), and for CD4-IML it was  $9.57 \pm 5.26$  mv (**Figure 2D**). Magnetic saturation curve analysis demonstrated that CD8-IML and CD4-IML possessed high saturation magnetization strengths and displayed relatively good superparamagnetic properties (**Figure 2E**). AFM observations of CD8-IML and CD4-IML are presented in **Figure 2F** that indicates that the seeded magnetic spheres were spherical in size without agglomeration. FT-IR spectroscopic tests (**Figure 2G**) indicated a new peak at approximately  $2,840\text{-}2,930$   $\text{cm}^{-1}$  that is due to the long carbon chains and methyl groups on the quaternary ammonium salt. The presence of GHDC on both IMLs indirectly suggested that the antibody was coupled to the surface of the magnetic sphere. The results of UV testing demonstrated that several immunomagnetic spheres exhibited a broad absorption peak at approximately 280 nm, whereas no UV absorption peak was observed for the IMLs, indicating that the antibodies were coupled to the surface of the spheres (**Figure 2H**).

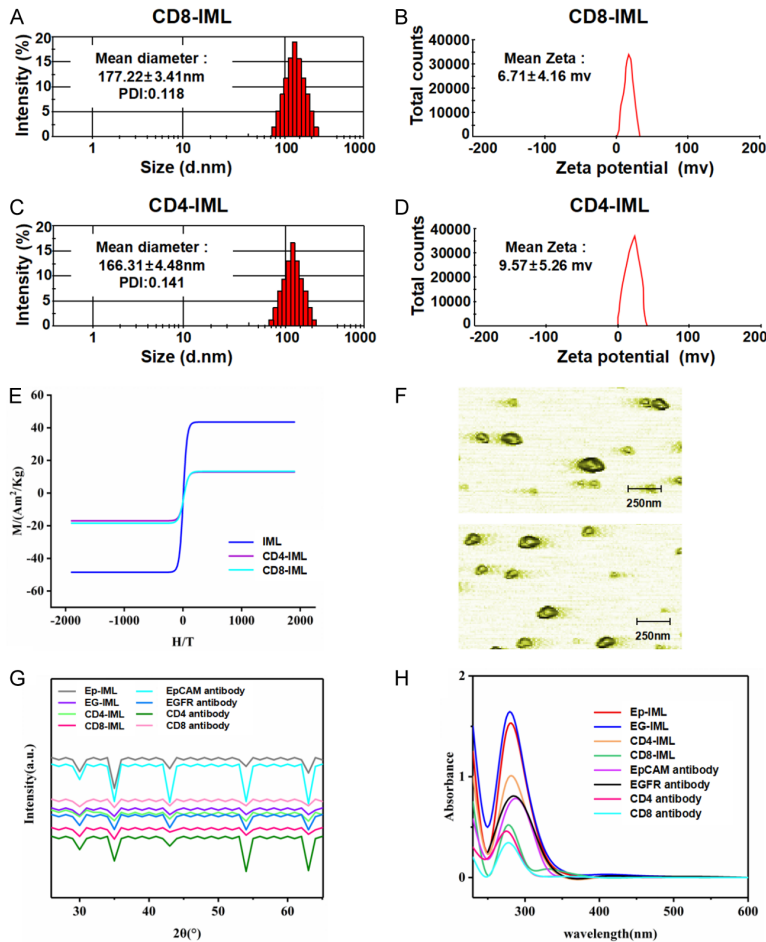


**Figure 2.** Characterization of the properties of antibody-modified magnetic nanospheres. A. CD8-IML particle size distribution. B. CD8-IML potential distribution. C. CD4-IML particle size distribution. D. CD4-IML potential distribution. E. Magnetic saturation curve analysis of the immunolipid magnetic spheres. F. AFM plots of CD8-IML and CD4-IML. G. FT-IR spectra of the immunolipid magnetic spheres. H. Ultraviolet absorption spectra of different IMLs.

*Analysis of the capture efficiency of magnetic spheres on cells*

Fluorescence microscopy images of different target magnetic spheres combined with three different head, neck, and throat tumor cell lines (HNE1, FaDu, and Hep-2) are presented in **Figure 3**. It was observed that different IMLs could automatically search for tumor cells in solution and adhere to the cell surfaces. An increased number of immunomagnetic beads gradually aggregated around the tumor cells, and after some time, the entire cell surface was surrounded by a sufficient number of magnetic vesicles. The binding of the immunomagnetic beads to different head and neck cancer cells increased with time until the magnetic vesicles

no longer adhered to the cell surface (**Figure 3A-C**). Cell capture efficiency analysis of the three nanolipid magnetic beads in three tumor cells demonstrated that the capture ability of all three IMLs was higher in phosphate buffered saline (PBS, 0.1 mol/l) than it was in blood. Among the three IMLs, Ep-IML exhibited the best capture capacity, and among the three tumor cells, the most significant effect was observed in FaDu and HNE1 cells (**Figure 3D, 3E**).

*Analysis of captured CTCs*

The collected peripheral blood samples were analyzed using established IMLs for the sorting and identification of tumor cells. Ep-IML, Vi-IML, and EG-IML were used to capture CTCs from the blood sample aliquots. Captured CTCs were identified and characterized using fluorescence microscopy. The results confirmed that the number of CTCs captured by the Ep-IML was the highest, and this was followed by that captured by the Vi-IML. EG-IML captured the lowest number of CTCs

(**Figure 4A**). On this basis, the addition of CD8 and CD4 IMLs for T lymphocyte enrichment was continued, and the results revealed that CD8 and CD4 possessed a high T lymphocyte enrichment ability that is important for diverse typing analyses in clinical diagnosis (**Figure 4B**). Additionally, both PBS and blood samples were selected for capture efficacy analysis of the five magnetic beads in this project, and the results indicated that Ep-IML exhibited the highest CTC sorting efficiency, followed by Vi-CTC and EG-CTC. CD8-IML and CD4-IML exhibited a similar capture ability for T cells, indicating that they possess a similar capture ability for T lymphocytes in peripheral blood. (**Figure 4C, 4D**).

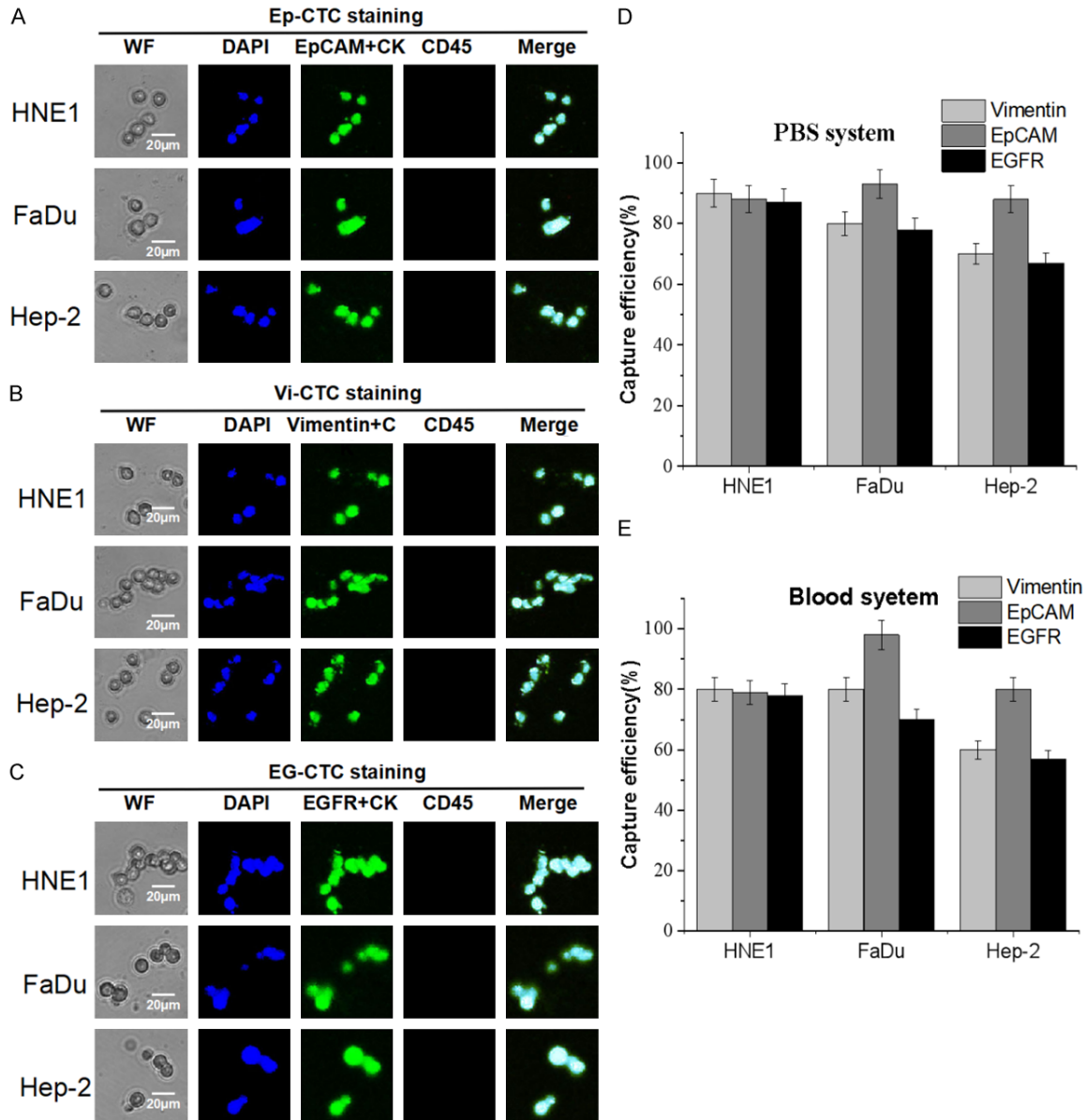


**Figure 3.** Cell capture efficiency experiment of different magnetic spheres. Fluorescence microscope images of Ep-IML (A), Vi-IML (B), and EG-IML (C) bound to cells. (D) Capture efficiency analysis in PBS (D) and blood (E) samples.

*CTC-derived PD-L1 positivity analysis*

After sorting and identifying peripheral blood CTCs from clinical samples, we selected samples positive for PD-L1 expression for further determination of CTC quantity. Positive enrichment for epithelial (EpCAM PD-L1+), mesenchymal (Vimentin PD-L1+), and EGFR+ (PD-L1+) cells demonstrated that PD-L1+-type Ep-CTCs captured the most cells, and PD-L1+-type Vi-CTCs and PD-L1+-type EG-CTC captured similar amounts (**Figure 5B**). Additionally, represen-

tative pictures of PD-L1+ versus PD-L1- are presented in **Figure 5A**. PD-L1 protein expression was defined as the percentage of positive membrane staining, and PD-L1(+) staining was defined as the average PD-L1 intensity above the cut-off (determined by summing the negative control and background intensities). PD-L1(+) staining was significantly stronger in fully circumferential or partially linear plasma membrane than it was in cytoplasmic staining. This suggests that epithelial, mesenchymal, and EGFR antibody-modified nanomagnetic

CTCs and PD-L1 in laryngopharyngeal head and neck tumors

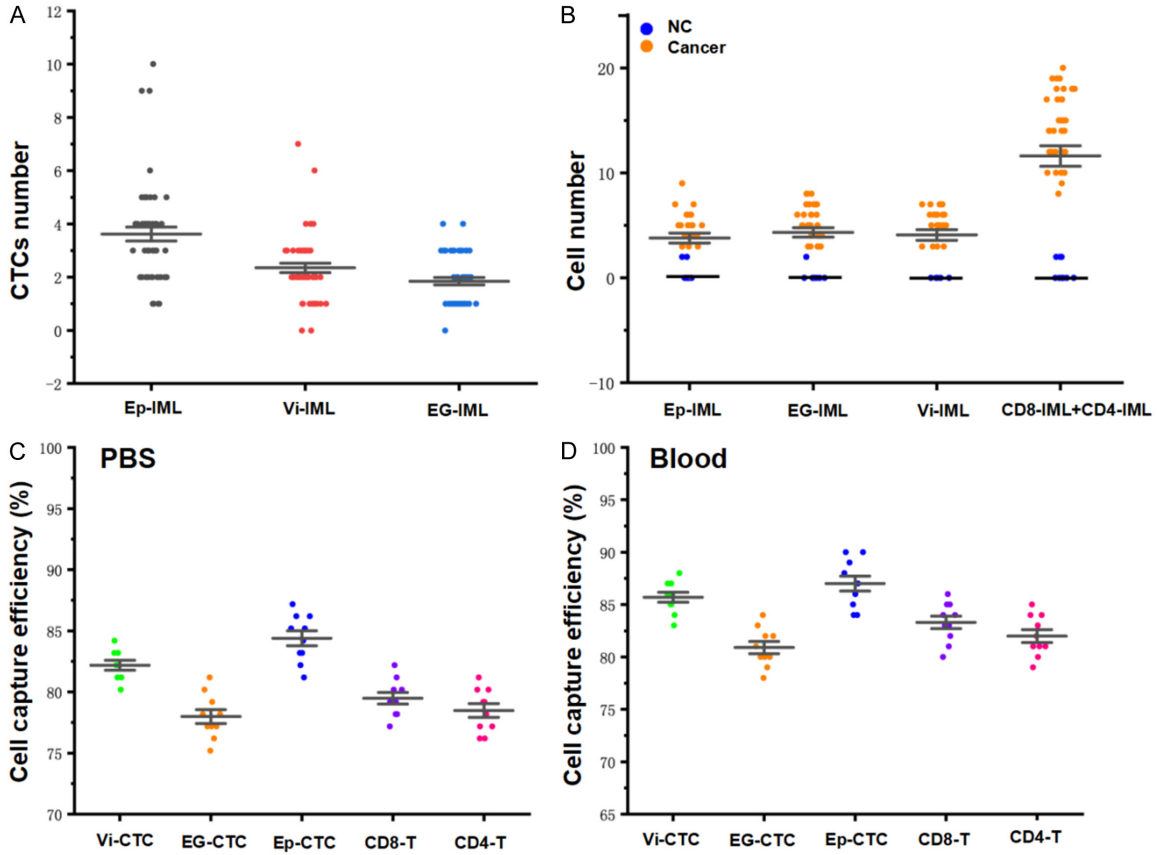


**Figure 4.** CTC counting and identification of clinical samples. (A) CTC capture ability of Ep-IML, Vi-IML, and EG-IML. (B) CTC capture after addition of CD8 and CD4 for T lymphocytes. Capture ability of Ep-IML, Vi-IML, EG-IML, CD8-IML, and CD4-IML in PBS (C) and blood (D) samples.

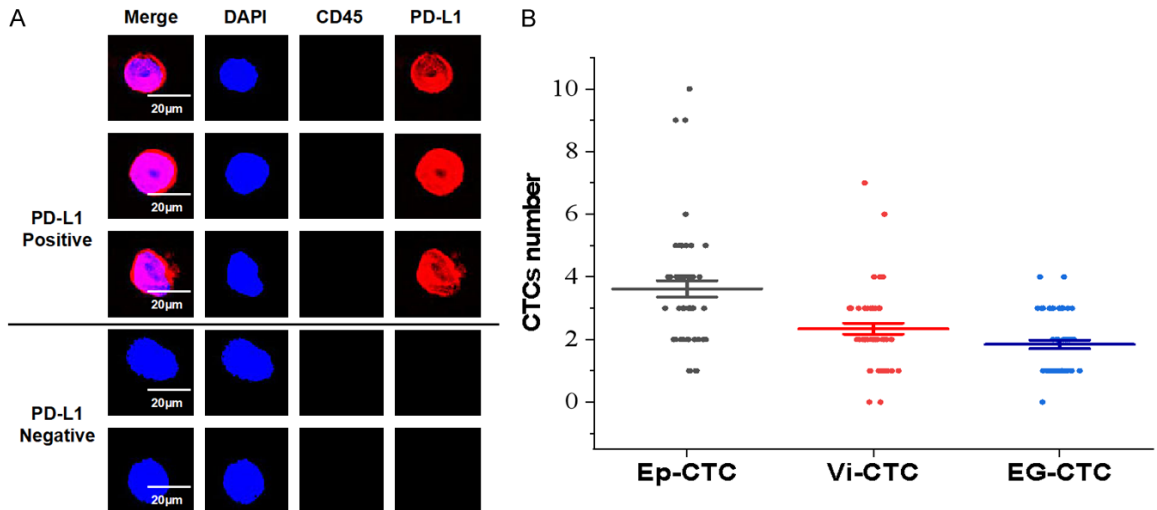


**Figure 5.** CTC counting and identification of clinical samples. A. Representative maps of PD-L1-positive and PD-L1-negative staining patterns. B. PD-L1+ type Ep-CTC, PD-L1+ type Vi-CTC, and PD-L1+ type EG-CTC capture analysis.

beads can be used to capture PD-L1 expressing CTCs more comprehensively and with high-

er sensitivity. The information carried by these CTCs is of great significance for the subsequent

## CTCs and PD-L1 in laryngopharyngeal head and neck tumors

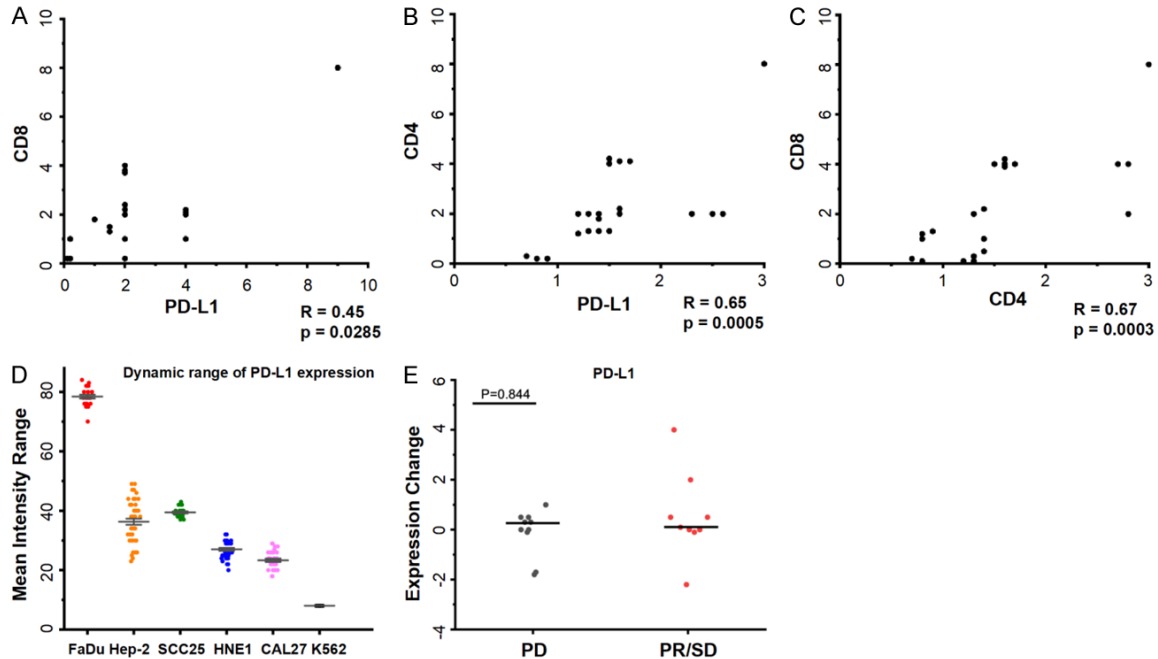


**Figure 6.** Correlation analysis of PD-L1-positive CTC with CD8/CD4 T cells. A. Correlation analysis of PD-L1+ CTC number with CD8+ T cells. B. Correlation analysis of PD-L1+ CTC number with CD4+ T cells. C. Correlation analysis of CD8+ with CD4+ T cells. D. Measurement of PD-L1 expression in pharyngeal head and neck tumor cell lines. E. Measurement of PD-L1 expression in PD and PR/SD samples.

exploration of tumor markers and the interpretation of EMT and malignant metastasis of tumors.

### Correlation analysis of PD-L1 with CD8/CD4

Based on the above measurements of PD-L1 and CD8/CD4 in clinical samples collected from pharyngeal head and neck tumors, we subsequently performed a correlation analysis between PD-L1 and CD8/CD4 to reveal the relationship between PD-L1 and CD8/CD4 in pharyngeal head and neck tumors. The results revealed a positive correlation between PD-L1 and CD8 (**Figure 6A**) and a negative correlation with CD4 (**Figure 6B**). CD8 and CD4 counts were negatively correlated for CTC counts (**Figure 6C**). We analyzed whether there was a difference in PD-L1 expression between the PD and PR/SD sample populations, and the results indicated no significant difference in PD-L1 expression between the PD and PR/SD samples (**Figure 6E**). Additionally, PD-L1 expression was assayed in the pharyngeal head and neck tumor cell lines, and the results revealed upregulated expression of PD-L1 in the pharyngeal head and neck tumor cell lines compared to levels in control K562 cells (**Figure 6D**).

### Effectiveness prediction and ROC analysis of this CTCs sorting system

Some of the samples underwent multiple dynamic peripheral blood sample collections at multiple time points and were used to analyze the role played by CTC in the treatment process and for efficacy evaluation. The results demonstrated that samples with high CTC counts exhibited a poor prognosis (**Figure 7A**). After treatment, CTC counts decreased, and samples with high CTC counts still exhibited a poorer prognosis than that of those with low CTC counts (**Figure 7B**). Based on the above data, the utility of CTC for dynamic monitoring was determined, and the AUC curve was plotted using ROC analysis. The obtained AUC value was 0.887 (**Figure 7C**). Typically, an AUC value of higher than 0.7 is considered to possess clinical value, confirming that CTC is valuable for clinical efficacy monitoring and prognostic evaluation. A higher number of CTCs in a single sample resulted in a higher possible risk index (**Figure 7D**).

### Analysis of PD-L1-related immune indexes

CTCs positive for PD-L1 expression in patient samples are presented in **Figure 8A**. It can be

## CTCs and PD-L1 in laryngopharyngeal head and neck tumors

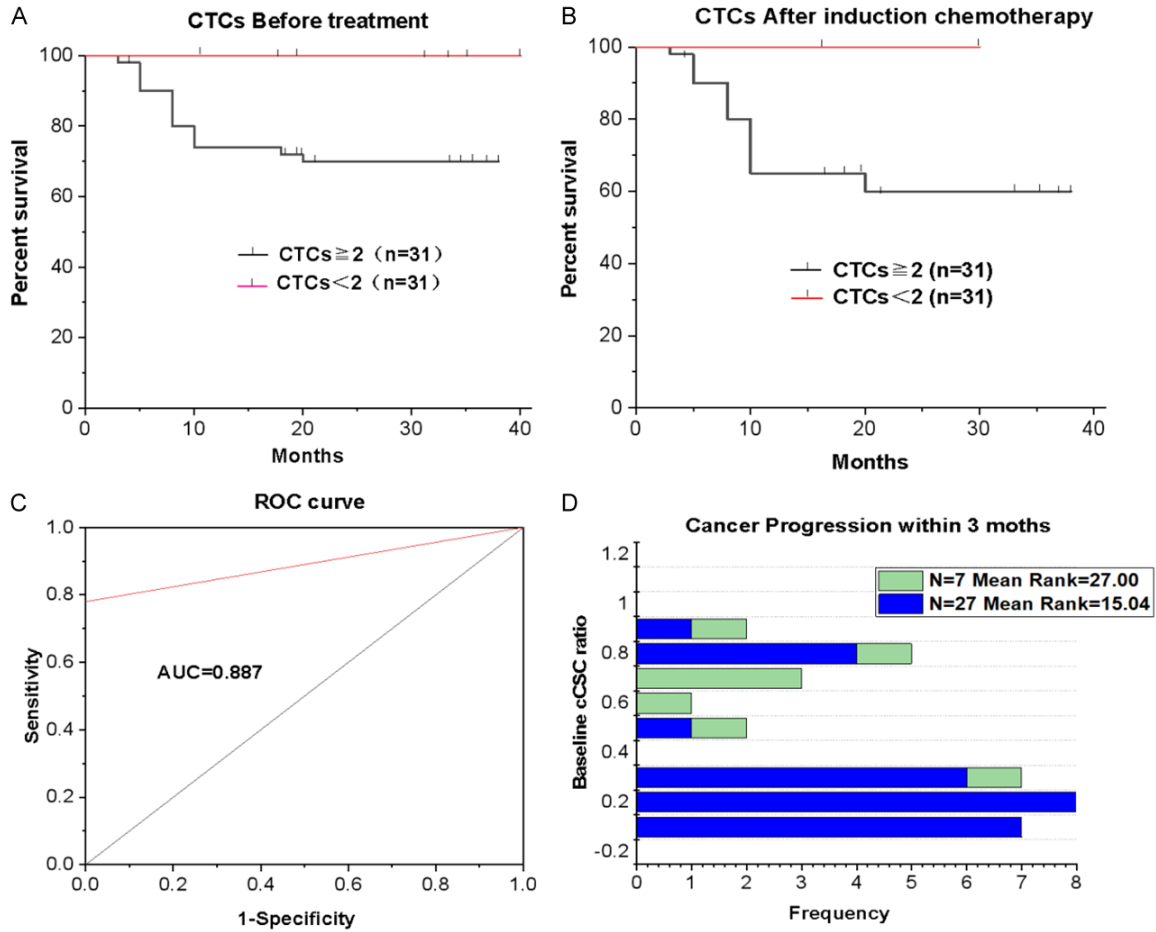


**Figure 7.** Effectiveness prediction and ROC analysis of this sorting system. A. Before treatment, analysis of the number of CTCs versus prognosis. B. After treatment, analysis of the number of CTCs versus prognosis. C. ROC analysis. D. Number of CTCs predicting the risk index.

observed from the figure that the expression of PD-L1 in CTCs with different phenotypes was consistent. The sorted CTCs exhibited obvious cell morphology features, were enriched with black nanomagnetic spheres, and expressed CK (green fluorescence) and PD-L1 (red fluorescence) simultaneously. At the cellular level, we analyzed the target adsorption recognition ability. The pharyngeal tumor cell lines HNE1, FaDu, and Hep-2 were mixed with magnetic beads. Different IMLs automatically searched for and adhered to tumor cells when they were mixed ([Supplementary Figure 2](#)). The increasing number of immunomagnetic beads gradually aggregated around the CTCs, and after some time, the cell surface was surrounded by a sufficient number of magnetic vesicles that increased with time until the magnetic vesicles no longer adhered to the cell surface. Additionally, at the cell line level, PD-L1 expres-

sion assays and validation experiments focused on the role of the effect on cytokine expression were performed. FaDu cells were first treated with a PD-L1 inhibitor and then co-cultured with T cells. The culture supernatant exhibited a significant increase in TNF- $\alpha$  levels and a significant decrease in IL-10 levels when tested with ELISA ([Figure 8B-D](#)).

### Discussion

In this study, a CTC capture system based on nanomaterials was developed from the peripheral blood of patients with head, neck, and throat tumors. This system is very effective for CTC capture, with a high capture efficiency and low cytotoxicity [37], thus making it an efficient and safe nanocarrier for targeted therapy. The addition of CD8 and CD4 nano-magnetic bead systems, the joint use of which exhibits a higher

## CTCs and PD-L1 in laryngopharyngeal head and neck tumors

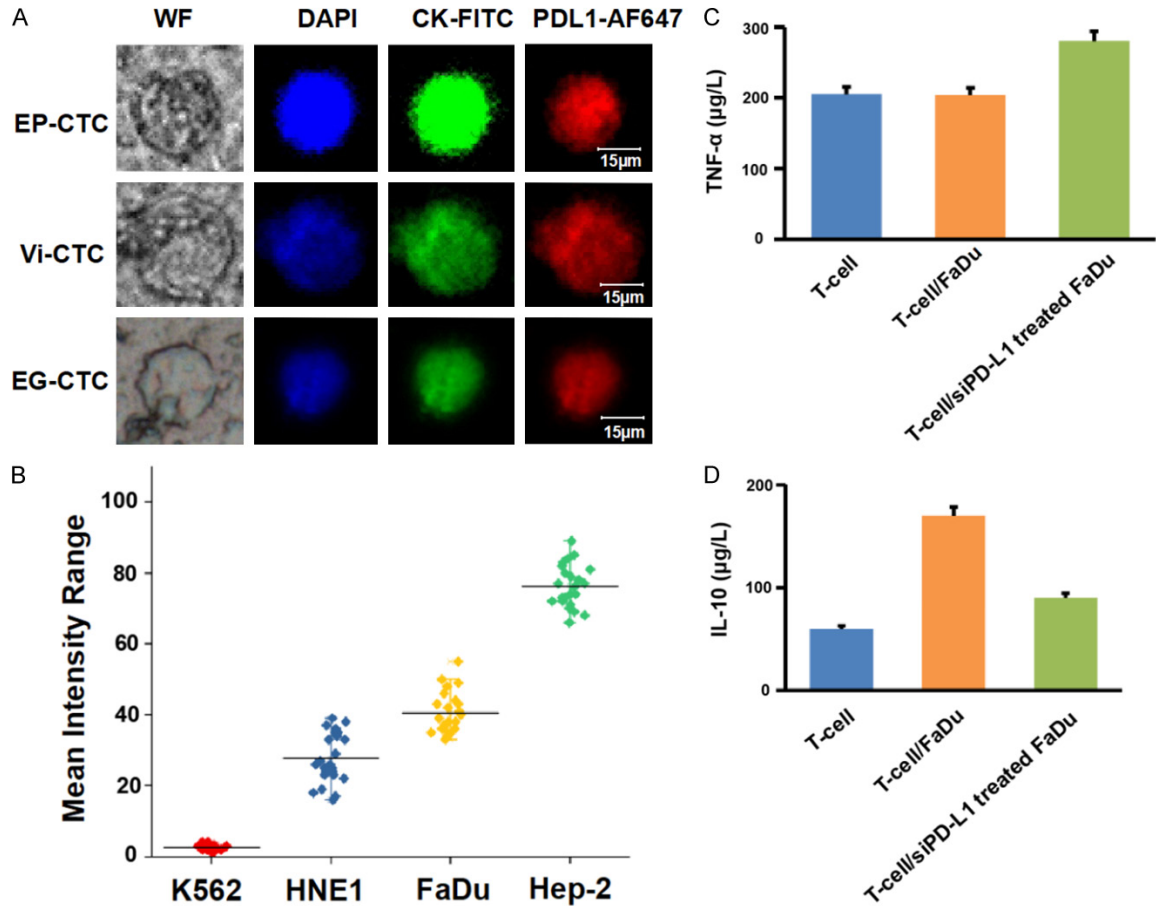


**Figure 8.** Image analysis of different phenotypes CTCs and their relationship with serum markers. (A) Fluorescence microscope images of different phenotypes of CTC with positive PD-L1 expression in the blood of patients. (B) Analysis of PD-L1 expression at different cell level. Measurement of inhibition of PD-L1 expression on the expression of the cytokines TNF- $\alpha$  (C) and IL-10 (D).

CTC capture capacity and confirms a very high correlation with PD-L1, is an effective aid for clinical dynamic monitoring. Strati A. et al. at the University of Athens reported that the expression of PD-L1 in CTC can provide feasible and important prognostic information for patients with head and neck squamous cell carcinoma. After treatment, patients whose CTCs overexpressed PD-L1 exhibited shorter progression-free survival ( $P=0.001$ ) and overall survival ( $P < 0.001$ ) [38]. Through the analysis of PD-L1 expression at the protein level, changes in CTC in PD-L1 positive patients can be further determined, and this plays an auxiliary role in clinical diagnosis and can be used as a dynamic detection index for the course of head, neck, and throat tumor treatment and as a predictor of recurrence risk. Some samples in which the tissues that were not positive for PD-L1 exhibited positive CTC levels of PD-L1 in

different subtypes, and this can exert a complementary effect. Additionally, in the presence of PD-L1 inhibition, monitoring revealed increased levels of the cytokine TNF- $\alpha$  and decreased levels of IL-10.

The limited predictive value of PD-L1 expression in primary tissues and the weak correlation between matched primary tumors and distant metastases suggest that primary tumors are not suitable alternatives for detecting PD-L1 expression at the metastatic site [39-41]. Magnetic beads were constructed by combining vimentin and EGFR antibody modifications in addition to the EpCAM single antibody-modified magnetic beads reported by CellSearch, aiming to capture CTCs from patients with laryngeal cancer and characterize the expression of PD-L1 [42-44]. Immunohistochemical assays are used to detect the

presence of the PD-L1 protein in tumor tissues to aid in clinical treatment decisions by identifying the PD-1/PD-L1 antibody regimen most likely to target tumors [45]. Additionally, PD-L1 is expressed in the tumor cells of many important cancer types, even in immune cells, and PD-L1 is also expressed in many components such as the cytoplasm or cell membrane, with wide variations in the expression levels of individual cells [46-48]. Therefore, measurement of PD-L1 expression by CTCs complements tissue PD-L1 analysis and assists in the development of clinical protocols.

This project established a high-precision CTC isolation and detection system for patients with pharyngeal tumors based on the CellSearch system that is based on the EpCAM/Vimentin/EGFR immunomagnetic sphere-positive sorting method for CTCs in patients with pharyngeal tumors [45]. It also incorporates for the first time two immune-related indicators, CD8 and CD4 that are comprehensive CTC capture systems. We performed analyses of PD-L1 that have also been rarely reported in studies focused on laryngeal cancer. Currently, our analysis includes only a small number of cases, and this is a shortcoming of this study. We will consider utilizing a larger sample size in subsequent studies to provide more theoretical support and a broader data base for clinical studies investigating this system.

### Acknowledgements

This study was supported by Natural Science Foundation of Fujian Province (Grant numbers: 2021J01784), Fujian provincial health technology project (Grant numbers: 2021GGAO17) and Double high-level medical institution construction fund of Fujian Province (2021-76).

Written informed consent was obtained from the patients enrolled in the study.

### Disclosure of conflict of interest

None.

**Address correspondence to:** Chen Li, Department of Otolaryngology, Fujian Medical University Union Hospital, No. 29, Xinquan Road, Fuzhou 350001, Fujian, China. E-mail: lichen0580@fjmu.edu.cn

### References

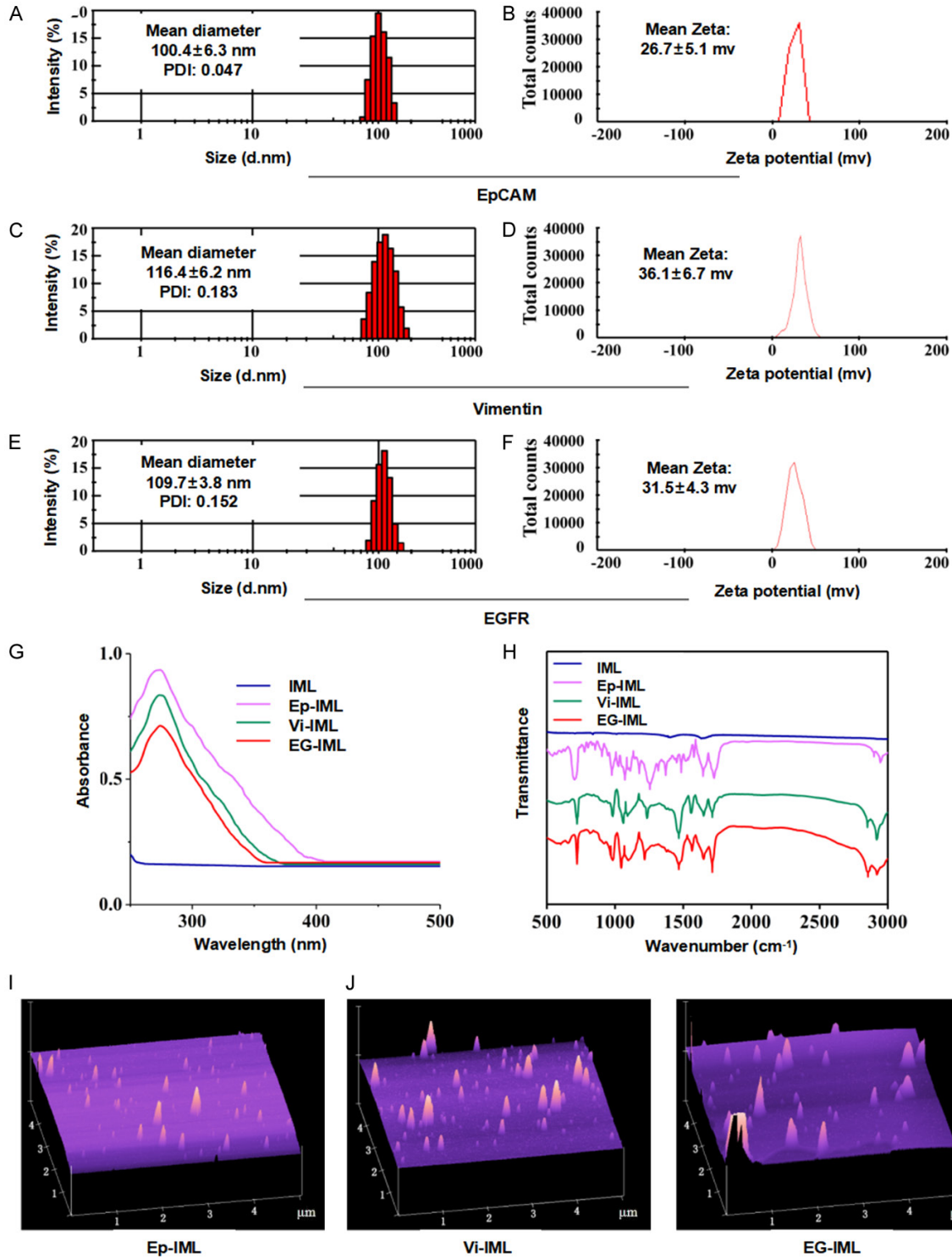
- [1] Mesia R, Iglesias L, Lambea J, Martínez-Trufero J, Soria A, Taberna M, Trigo J, Chaves M, García-Castaño A and Cruz J. SEOM clinical guidelines for the treatment of head and neck cancer (2020). *Clin Transl Oncol* 2021; 23: 913-921.
- [2] Hashim D, Genden E, Posner M, Hashibe M and Boffetta P. Head and neck cancer prevention: from primary prevention to impact of clinicians on reducing burden. *Ann Oncol* 2019; 30: 744-756.
- [3] Zhang Y and Zhang Z. The history and advances in cancer immunotherapy: understanding the characteristics of tumor-infiltrating immune cells and their therapeutic implications. *Cell Mol Immunol* 2020; 17: 807-821.
- [4] Gutwillig A, Santana-Magal N, Farhat-Younis L, Rasoulouniriana D, Madi A, Luxenburg C, Cohen J, Padmanabhan K, Shomron N, Shapira G, Gleiberman A, Parikh R, Levy C, Feinmesser M, Hershkovitz D, Zemser-Werner V, Zlotnik O, Kroon S, Hardt WD, Debets R, Reticker-Flynn NE, Rider P and Carmi Y. Transient cell-in-cell formation underlies tumor relapse and resistance to immunotherapy. *Elife* 2022; 11: e80315.
- [5] Jiménez-Chávez ÁJ and Moreno-Fierros L. Non-enveloped virus-like particles: a promising antigen-delivery strategy for the induction of anti-tumor immune responses. *Nano Life* 2022; 12: 2230004.
- [6] Zhang Q, Zhang M and Wang W. Construction of shikonin-loaded mammaglobin-modified liposomes for breast cancer targeted therapy. *Nano Life* 2022; 12: 2250010.
- [7] Zekan DS, Dahman A, Hajiran AJ, Luchey AM, Chahoud J and Spiess PE. Prognostic predictors of lymph node metastasis in penile cancer: a systematic review. *Int Braz J Urol* 2021; 47: 943-956.
- [8] Zhang S, Zhang Y, Feng Y, Wu J, Hu Y, Lin L, Xu C, Chen J, Tang Z, Tian H and Chen X. Biomimetic two-enzyme nanoparticles regulate tumor glycometabolism inducing tumor cell pyroptosis and robust antitumor immunotherapy. *Adv Mater* 2022; 34: e2206851.
- [9] O'Donnell JS, Teng MWL and Smyth MJ. Cancer immunoeediting and resistance to T cell-based immunotherapy. *Nat Rev Clin Oncol* 2019; 16: 151-167.
- [10] Duan X, Chan C and Lin W. Nanoparticle-mediated immunogenic cell death enables and potentiates cancer immunotherapy. *Angew Chem Int Ed Engl* 2019; 58: 670-680.
- [11] Bagchi S, Yuan R and Engleman EG. Immune checkpoint inhibitors for the treatment of can-

- cer: clinical impact and mechanisms of response and resistance. *Annu Rev Pathol* 2021; 16: 223-249.
- [12] Tayoun T, Faugeron V, Oulhen M, Aberlenc A, Pawlikowska P and Farace F. CTC-derived models: a window into the seeding capacity of circulating tumor cells (CTCs). *Cells* 2019; 8: 1145.
- [13] Pipatwatcharadate C, Iyer PR and Pissuwan D. Recent update roles of magnetic nanoparticles in circulating tumor cell (CTC)/non-CTC separation. *Pharmaceutics* 2023; 15: 2482.
- [14] Fernández-Santiago C, López-López R and Piñeiro R. Models to study CTCs and CTC culture methods. *Int Rev Cell Mol Biol* 2023; 381: 57-98.
- [15] Descamps L, Le Roy D and Deman AL. Microfluidic-based technologies for CTC isolation: a review of 10 years of intense efforts towards liquid biopsy. *Int J Mol Sci* 2022; 23: 1981.
- [16] Sulaiman R, De P, Aske JC, Lin X, Dale A, Vaseelaar E, Koirala N, Ageton C, Gaster K, Plorde J, Solomon B, Thaemert B, Meyer P, Espaillet LR, Starks D and Dey N. A laboratory-friendly CTC identification: comparable double-immunocytochemistry with triple-immunofluorescence. *Cancers (Basel)* 2022; 14: 2871.
- [17] Li T, Xu S, Wang Y, Wei Y, Shi L, Xiao Z, Liu Z, Deng WW and Ning J. Quality chemical analysis of crush-tear-curl (CTC) black tea from different geographical regions based on UHPLC-Orbitrap-MS. *J Food Sci* 2021; 86: 3909-3925.
- [18] Deutsch TM, Stefanovic S, Feisst M, Fischer C, Riedel F, Fremd C, Domschke C, Pantel K, Hartkopf AD, Sutterlin M, Brucker SY, Schneeweiss A and Wallwiener M. Cut-off analysis of CTC change under systemic therapy for defining early therapy response in metastatic breast cancer. *Cancers (Basel)* 2020; 12: 1055.
- [19] Bath IS, Mitra A, Rood S, Kopetz S, Menter D and Li S. CTC analysis: an update on technological progress. *Transl Res* 2019; 212: 14-25.
- [20] Zhou X, Luo B, Kang K, Zhang Y, Jiang P, Lan F, Yi Q and Wu Y. Leukocyte-repelling biomimetic immunomagnetic nanoplatform for high-performance circulating tumor cells isolation. *Small* 2019; 15: e1900558.
- [21] Singh S, Pathak A, Kumar S, Malik PS and Elangovan R. Rapid immunomagnetic co-capture assay for quantification of lung cancer associated exosomes. *J Immunol Methods* 2022; 508: 113324.
- [22] Chakiryan NH, Dahmen A, Cucchiara V, Briganti A, Montorsi F, Salonia A, Spiess PE and Necchi A. Reliability of serum tumor marker measurement to diagnose recurrence in patients with clinical stage I nonseminomatous germ cell tumors undergoing active surveillance: a systematic review. *J Urol* 2021; 205: 1569-1576.
- [23] Salzmann M, Enk AH and Hassel JC. S100 as serum tumor marker in advanced uveal melanoma. *Biomolecules* 2023; 13: 529.
- [24] Nam H, Hong SS, Jung KH, Kang S, Park MS, Kang S, Kim HS, Mai VH, Kim J, Lee H, Lee W, Suh YJ, Lim JH, Kim SY, Kim SC, Kim SH and Park S. A serum marker for early pancreatic cancer with a possible link to diabetes. *J Natl Cancer Inst* 2022; 114: 228-234.
- [25] Larionova I, Tuguzbaeva G, Ponomaryova A, Stakheyeva M, Cherdyntseva N, Pavlov V, Choinzonov E and Kzhyshkowska J. Tumor-associated macrophages in human breast, colorectal, lung, ovarian and prostate cancers. *Front Oncol* 2020; 10: 566511.
- [26] Heidrich I, Aćkar L, Mossahebi Mohammadi P and Pantel K. Liquid biopsies: potential and challenges. *Int J Cancer* 2021; 148: 528-545.
- [27] Berrian J, Liu Y, Ezenwajiaku N, Moreno-Aspitia A, Holton SJ, Toriola AT, Colditz GA, Houston AJ, Hall L, Fiala MA and Ademuyiwa FO. Impact of the COVID-19 pandemic on breast, colorectal, lung, and prostate cancer stage at diagnosis according to race. *Cancer Med* 2023; 12: 7381-7388.
- [28] Yi M, Niu M, Xu L, Luo S and Wu K. Regulation of PD-L1 expression in the tumor microenvironment. *J Hematol Oncol* 2021; 14: 10.
- [29] Cha JH, Chan LC, Li CW, Hsu JL and Hung MC. Mechanisms controlling PD-L1 expression in cancer. *Mol Cell* 2019; 76: 359-370.
- [30] Wang J, Xu Y, Rao X, Zhang R, Tang J, Zhang D, Jie X, Zhu K, Wang X, Xu Y, Zhang S, Dong X, Zhang T, Yang K, Xu S, Meng R and Wu G. BRD4-IRF1 axis regulates chemoradiotherapy-induced PD-L1 expression and immune evasion in non-small cell lung cancer. *Clin Transl Med* 2022; 12: e718.
- [31] Jiang Y, Yuan Y, Chen M, Li S, Bai J, Zhang Y, Sun Y, Wang G, Xu H, Wang Z, Zheng Y and Nie H. PRMT5 disruption drives antitumor immunity in cervical cancer by reprogramming T cell-mediated response and regulating PD-L1 expression. *Theranostics* 2021; 11: 9162-9176.
- [32] Chen S, Crabill GA, Pritchard TS, McMiller TL, Wei P, Pardoll DM, Pan F and Topalian SL. Mechanisms regulating PD-L1 expression on tumor and immune cells. *J Immunother Cancer* 2019; 7: 305.
- [33] Peng QH, Wang CH, Chen HM, Zhang RX, Pan ZZ, Lu ZH, Wang GY, Yue X, Huang W and Liu RY. CMTM6 and PD-L1 coexpression is associated with an active immune microenvironment and a favorable prognosis in colorectal cancer. *J Immunother Cancer* 2021; 9: e001638.
- [34] Sun L, Huang C, Zhu M, Guo S, Gao Q, Wang Q, Chen B, Li R, Zhao Y, Wang M, Chen Z, Shen B and Zhu W. Gastric cancer mesenchymal stem cells regulate PD-L1-CTCF enhancing cancer

## CTCs and PD-L1 in laryngopharyngeal head and neck tumors

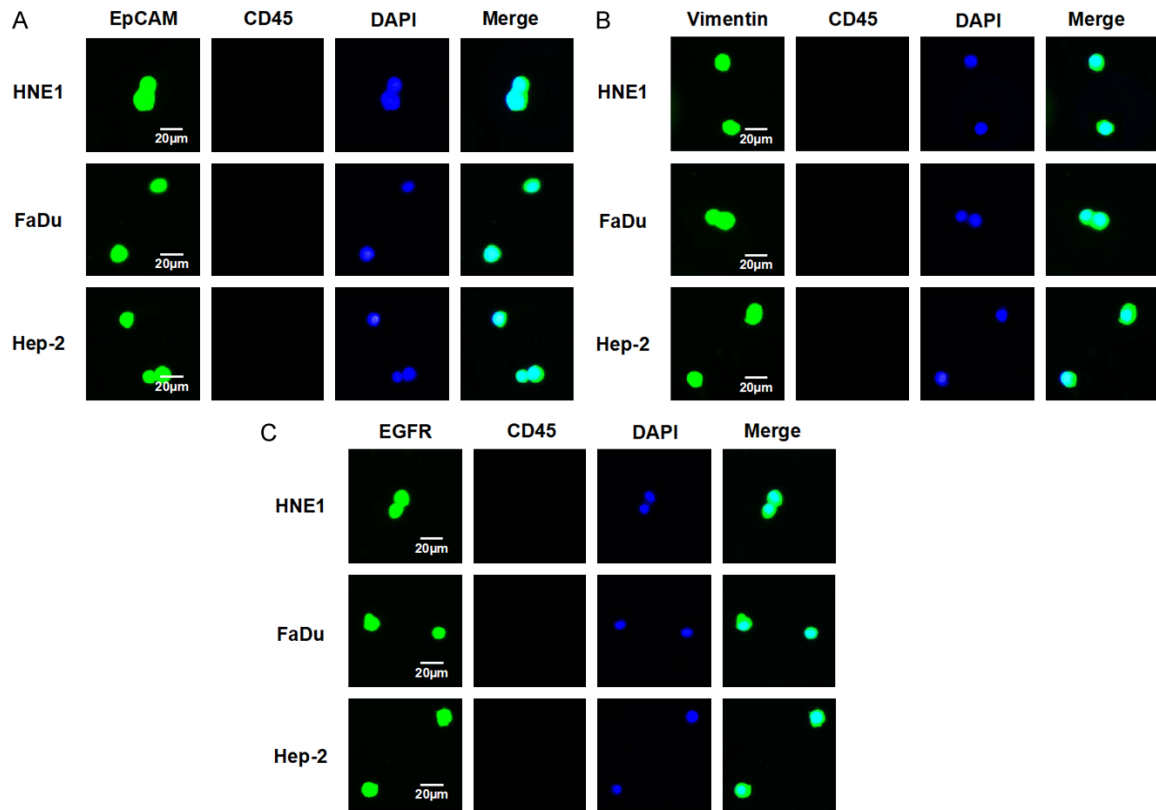
- stem cell-like properties and tumorigenesis. *Theranostics* 2020; 10: 11950-11962.
- [35] Chao YC, Lee KY, Wu SM, Kuo DY, Shueng PW and Lin CW. Melatonin downregulates PD-L1 expression and modulates tumor immunity in KRAS-mutant non-small cell lung cancer. *Int J Mol Sci* 2021; 22: 5649.
- [36] Almici C, Neva A, Skert C, Bruno B, Verardi R, Di Palma A, Bianchetti A, Braga S, Piovani G, Cancelli V, Omedè P, Baeten K, Rotta G, Russo D and Marini M. Counting circulating endothelial cells in allo-HSCT: an ad hoc designed polychromatic flowcytometry-based panel versus the CellSearch System. *Sci Rep* 2019; 9: 87.
- [37] Yi B, Wu T, Zhu N, Huang Y, Yang X, Yuan L, Wu Y, Liang X and Jiang X. The clinical significance of CTC enrichment by GPC3-IML and its genetic analysis in hepatocellular carcinoma. *J Nanobiotechnology* 2021; 19: 74.
- [38] Strati A, Koutsodontis G, Papaxoinis G, Angelidis I, Zavridou M, Economopoulou P, Kotsantis I, Avgeris M, Mazel M, Perisanidis C, Sasaki C, Alix-Panabières C, Lianidou E and Psyrri A. Prognostic significance of PD-L1 expression on circulating tumor cells in patients with head and neck squamous cell carcinoma. *Ann Oncol* 2017; 28: 1923-1933.
- [39] Yao H, Lan J, Li C, Shi H, Brosseau JP, Wang H, Lu H, Fang C, Zhang Y, Liang L, Zhou X, Wang C, Xue Y, Cui Y and Xu J. Inhibiting PD-L1 palmitoylation enhances T-cell immune responses against tumours. *Nat Biomed Eng* 2019; 3: 306-317.
- [40] Ying H, Zhang X, Duan Y, Lao M, Xu J, Yang H, Liang T and Bai X. Non-cytoplasmic PD-L1: an atypical target for cancer. *Pharmacol Res* 2021; 170: 105741.
- [41] Hu X, Lin Z, Wang Z and Zhou Q. Emerging role of PD-L1 modification in cancer immunotherapy. *Am J Cancer Res* 2021; 11: 3832-3840.
- [42] Cohen EEW, Bell RB, Bifulco CB, Burtneiss B, Gillison ML, Harrington KJ, Le QT, Lee NY, Leidner R, Lewis RL, Licitra L, Mehanna H, Mell LK, Raben A, Sikora AG, Uppaluri R, Whitworth F, Zandberg DP and Ferris RL. The Society for Immunotherapy of Cancer consensus statement on immunotherapy for the treatment of squamous cell carcinoma of the head and neck (HNSCC). *J Immunother Cancer* 2019; 7: 184.
- [43] Hirshoren N, Al-Kharouf I, Weinberger JM, Eliashar R, Popovtzer A, Knaanie A, Fellig Y, Neuman T, Meir K, Maly A and Vainer GW. Spatial intratumoral heterogeneity expression of PD-L1 antigen in head and neck squamous cell carcinoma. *Oncology* 2021; 99: 464-470.
- [44] Overholser J, Guo L and Kaumaya PTP. Magnetic fluorescent bead-based dual-reporter flow analysis of PDL1-Vaxx peptide vaccine-induced antibody blockade of the PD-1/PD-L1 interaction. *J Vis Exp* 2023.
- [45] Xia L, Liu Y and Wang Y. PD-1/PD-L1 blockade therapy in advanced non-small-cell lung cancer: current status and future directions. *Oncologist* 2019; 24 Suppl 1: S31-S41.
- [46] Gao Y, Nihira NT, Bu X, Chu C, Zhang J, Kolodziejczyk A, Fan Y, Chan NT, Ma L, Liu J, Wang D, Dai X, Liu H, Ono M, Nakanishi A, Inuzuka H, North BJ, Huang YH, Sharma S, Geng Y, Xu W, Liu XS, Li L, Miki Y, Sicinski P, Freeman GJ and Wei W. Acetylation-dependent regulation of PD-L1 nuclear translocation dictates the efficacy of anti-PD-1 immunotherapy. *Nat Cell Bio* 2020; 22: 1064-1075.
- [47] Yin Z, Yu M, Ma T, Zhang C, Huang S, Karimzadeh MR, Momtazi-Borojeni AA and Chen S. Mechanisms underlying low-clinical responses to PD-1/PD-L1 blocking antibodies in immunotherapy of cancer: a key role of exosomal PD-L1. *J Immunother Cancer* 2021; 9: e001698.
- [48] Hong W, Xue M, Jiang J, Zhang Y and Gao X. Circular RNA circ-CPA4/let-7 miRNA/PD-L1 axis regulates cell growth, stemness, drug resistance and immune evasion in non-small cell lung cancer (NSCLC). *J Exp Clin Cancer Res* 2020; 39: 149.

# CTCs and PD-L1 in laryngopharyngeal head and neck tumors



**Supplementary Figure 1.** Material characterization of antibody modified immunolipid magnetic nano-beads. A, B. Size distribution and zeta distribution of Ep-IML. C, D. Size distribution and zeta distribution of Vi-IML. E, F. Size distribution and zeta distribution of EG-IML. G. Ultraviolet absorption spectrum of immunolipid magnetic nano-beads. H. FT-IR spectrum of immunolipid magnetic nano-beads. I-K. AFM image of Ep-IML, Vi-IML and EG-IML.

CTCs and PD-L1 in laryngopharyngeal head and neck tumors



**Supplementary Figure 2.** Analysis of cell (HNE1, FaDu, and HNE1) binding state with different IMLs. Targeted identification of laryngeal cancer cells for EpCAM (A), Vimentin (B) and EGFR (C), respectively.